Hindawi
Advances in Meteorology
Volume 2019, Article ID 8512727, 11 pages
https://doi.org/10.1155/2019/8512727

Research Article

Hydrological Drought Assessment of Energy-Based Water Deficit Index (EWDI) at Different Geographical Regions

Chanyang Sur,[1] Dongkyun Kim,[2] Joo-Heon Lee,[3] Muhammad Mazhar Iqbal,[4] and Minha Choi[4]

[1]*Drought Research Center, Joongbu University, Goyang, Gyeonggi, Republic of Korea*
[2]*Department of Civil Engineering, Hongik University, Seoul, Republic of Korea*
[3]*Department of Civil Engineering, Joongbu University, Goyang, Gyeonggi, Republic of Korea*
[4]*Department of Water Resources, Graduate School of Water Resources, Sungkyunkwan University, Suwon, Republic of Korea*

Correspondence should be addressed to Minha Choi; mhchoi@skku.edu

Received 29 November 2018; Revised 25 February 2019; Accepted 23 April 2019; Published 29 May 2019

Academic Editor: Giacomo Gerosa

This study applied the remote sensing-based drought index, namely, the Energy-Based Water Deficit Index (EWDI), across Mongolia, Australia, and Korean Peninsula for the period between 2000 and 2010. The EWDI is estimated based on the hydrometeorological variables such as evapotranspiration, soil moisture, solar radiation, and vegetation activity which are derived from the Moderate Resolution Imaging Spectroradiometer (MODIS) imageries. The estimated EWDI was compared with the Evaporative Stress Index (ESI), the Vegetation Condition Index (VCI), and the Standardized Precipitation Index (SPI). The correlation coefficients between the drought indices are as follows: 0.73–0.76 (EWDI vs ESI), 0.64–0.71 (EWDI vs VCI), 0.54–0.64 (EWDI vs SPI-3), 0.69–0.71 (ESI vs VCI), 0.55–0.62 (ESI vs SPI-3), and 0.53–0.57 (VCI vs SPI-3). The drought prediction accuracy of each index according to error matrix analysis is as follows: 83.33–94.17% (EWDI), 70.00–91.67% (ESI), 47.50–85.00% (VCI), and 61.67–88.33% (SPI-3). Based on the results, the EWDI and ESI were found to be more accurate in capturing moderate drought conditions than the SPI at different geographical regions.

1. Introduction

In general, drought is considered from numerous perceptions. Firstly, meteorological drought which is usually interpreted by degree of aridness and duration of aridness and its extent, which shows anomalies, correspond to cumulative precipitation. Secondly, hydrological drought is related to the precipitation deficits on water supply, which is quantified by short runoff, deepened ground water level, and water resource deficiencies. Thirdly, agriculture drought accounts for the variable susceptibility of vegetation during different statuses of vegetation development which is estimated by measuring diminution in crop yield and soil moistness as well as differences among actual and potential evapotranspiration.

Due to these assorted definitions of drought as well as troublesome in estimating the precise commencement, range, level, and end of drought, substantial efforts have been utilized to delineate techniques for investigation and monitoring of drought. However, the conventional drought has been considered based on the hydrometeorological variables measured by the network of in situ data tools, whereas remote sensing technology is robust substituted by providing decisive hydrometeorological variables for drought analysis at the enormously higher spatial scale than the capability of in situ network devices. Several studies have presented remote sensing-based drought indices. Likewise, Kogan [1] introduced the Vegetation Condition Index (VCI) by using remote sensing-based Normalized Difference Vegetation Index (NDVI) data, and Kogan [2] developed the Vegetation Health Index (VHI) by using remotely sensed data of TIR imageries to monitor variation in canopy temperatures. Anderson et al. [3–5] developed a new drought index known as "Evaporative Stress Index" (hereafter ESI). They assessed

the ESI crosswise the globe based on water vapor and temperature that is attained from the remote sensing model named "Atmosphere-Land Exchange Inverse (ALEXI) remote sensing model" [3–5]. They described that the ESI correlated soundly with the Palmer Drought Severity Index (PDSI) and Standardized Precipitation Index (SPI). Mu et al. [6] proposed the Drought Severity Index (DSI) which was based on MODIS data. Their proposed DSI matched well not only with the Palmer Drought Severity Index (PDSI) and Standardized Precipitation Index (SPI) but also with the vegetation net primary production (NPP) data which designated that the index was useful for assessing drought stimuli on crop production and forest growth. Keshavarz et al. [7] proposed and evaluated a new drought index, Soil Water Deficit Index (SWDI), to study the agricultural drought. Here, it is remarkable that almost all of these drought indices focus on specific aspects of various and complex drought conditions in reality. For example, SPI, ESI, EDI, and PDSI were estimated primarily based on meteorological variables, so these indices did not reflect the level of soil moisture that could mainly influence crop growth and ecology. Moreover, VHI and SWDI are mainly estimated based on other variables related to vegetative greening conditions, so they cannot accurately reveal the instant of meteorological phenomena that can improve drought severity. For tenacity of this issue, Sur et al. [8] assessed a progressive drought index named "Energy-Based Water Deficit Index" (EWDI), which concurrently considered the circulation of energy, water, and carbon across the soil surface and atmosphere to reflect the complex conditions of droughts related to atmosphere and vegetation. They estimated this index across Korean Peninsula using MODIS-based datasets and exposed that the EWDI performed well and showed favorable association with the ESI (correlation coefficient within 0.73 and 0.76 based on their specific study area) as well as the conventional drought indices such as PDSI (correlation coefficient within 0.57 and 0.67) and SPI (correlation coefficient within 0.61 and 0.64). As outcomes of their research were achieved based on the data of Korean Peninsula which is located on the northeastern brink of the Asian continent, they could not interpret an overall conclusion for the applicability and legitimacy of the EWDI on a wide range of spatial scales across the globe.

In this view, the main purpose of this research is to enhance the application of EWDI by validating the EWDI at other geographical locations with greater spatial scales that are prone to drought. To attain this goal, the EWDI, ESI, VCI, and SPI were estimated across Mongolia (north-central Asia), the Australian continent, and the remaining part of Korean Peninsula for the duration of 2000–2010. Linear regression and error matrices were used to compare estimated indices with each other.

2. Study Area and Datasets

2.1. Study Area

2.1.1. Mongolia. The first study area was the north-central Asian country Mongolia located between 42–51°N (latitude) and 85–120°E (longitude) (Figure 1). The total area of Mongolia is nearly 1.6 million square kilometers, and the elevation ranges from 1,000 m to 2,500 m above the mean sea level. The country is divided into six types of natural zones having different soil types and plant life in each zone. In this study, meteorological data are obtained from six selected stations which cover the entire country. The climate of Mongolia is described by a dry and hot summer, a long-lasting cold winter, high temperature variations, low precipitation, and a relatively high total of sunny days (on average 260 days per year) [9]. Mongolia, which is relatively a dry region, has a less mean annual precipitation, accumulating to approximately 100–200 mm in the dry southern mountainous regions and 200–350 mm in the northern mountainous regions [10]. The entire area has a total annual precipitation about 90 mm. The northern part of Mongolia is mountainous ranges characterized by dense forests in a dry subhumid climate, whereas the southern region is the Gobi Desert characterized by a drier climate at lower elevations [9]. The above-mentioned climatic array as a function of latitude also described the vegetation pattern athwart Mongolia.

2.1.2. Australia. The second study area was Australia located between 10–40°S (latitude) and 113–153°E (longitude) (Figure 1). The total area of Australia is 7,617,930 km^2 setting on the Indo-Australian Plate. Australia is separated into eight climate zones which are defined by the Building Code of Australia (BCA). Based on the local geographical varieties including wind patterns and elevation above the mean sea level, each climate zone is further subdivided into many subzones.

2.1.3. Korean Peninsula. Korean Peninsula is located on the northeast brink of Asia at 33–43°N (latitude) and 124–132°E (longitude) (Figure 1). Even though Korean Peninsula has been previously investigated by Sur et al. [8], this study presents the result of the additional analysis performed in the north Korean region. Korean Peninsula covers an area of 219,020 km^2, located in the Asian monsoon region, having a mean annual precipitation approximately 1,100 mm (North Korea, 919.7 mm; South Korea, 1,307.7 mm). The topography of the study area represents an elevation range about 0–1,915 m [11]. The land use is mainly composed of croplands (29.7%), mixed forests (39.6%), deciduous broadleaf forests (14.4%), woody savannas (6.3%), and residential and commercial areas (5.2%). Table 1 describes the geographical features of meteorological observations.

Validations of various drought indices were performed for the selected three meteorological measurement sites (Hamheung, Anju, and Kimchaek). The meteorological observation stations and flux tower are presented in Figure 1, and the features of each meteorological station are described in Table 1.

2.2. Datasets. In this study, to calculate drought indices, input datasets were obtained from the MODIS satellite and ground observation for the duration of 2000–2010. The

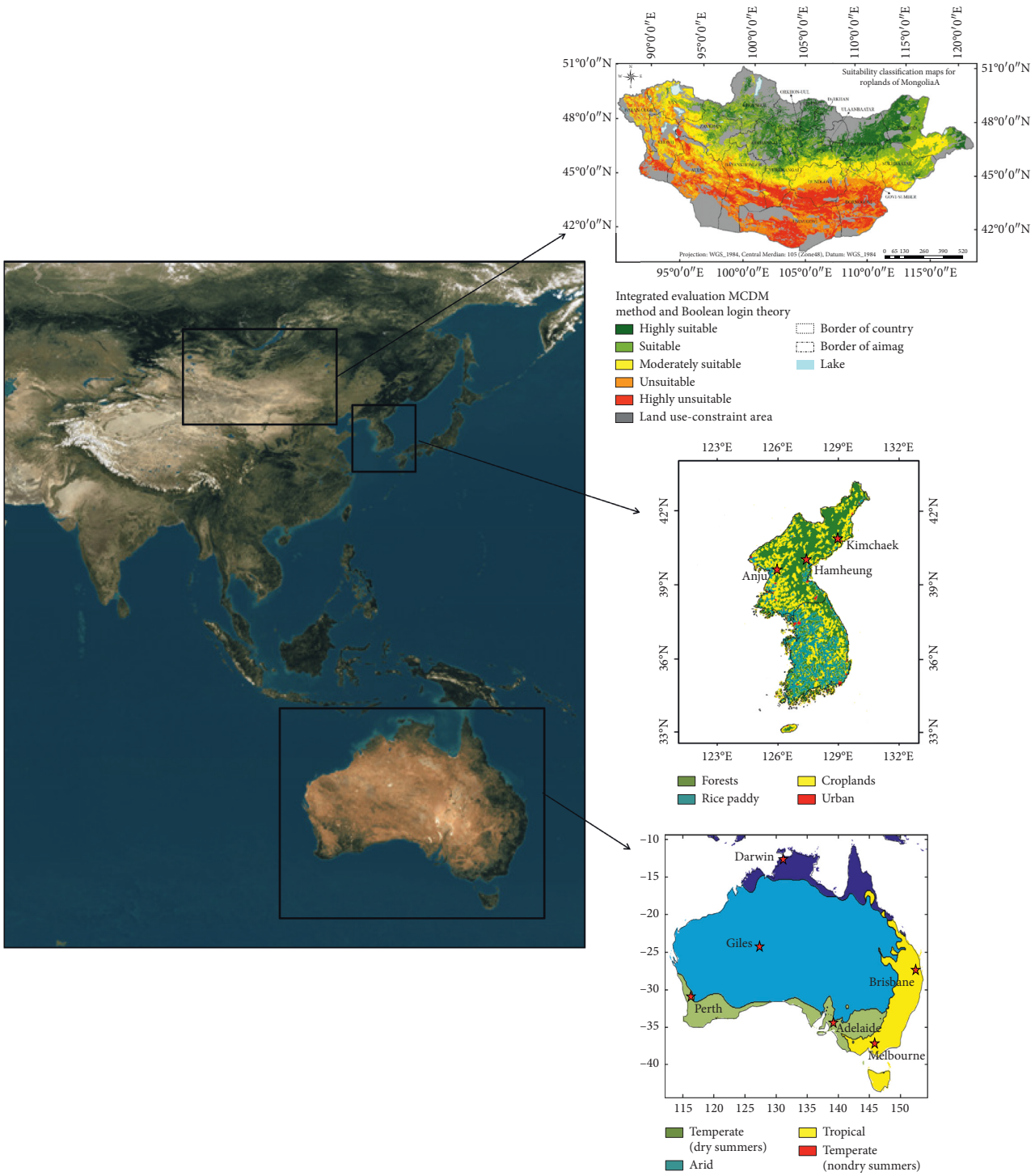

Figure 1: Geographical locations of study areas.

MODIS multispectral sensor that is the scientific instrument sent off into the earth circle by NASA's Earth Observing System (EOS) was developed to observe the atmosphere, land, and ocean. The temporal resolution is 1 day, and the spatial resolutions of the sensor estimations are 1 km, 500 m, and 250 m. The sensors are found on board the Terra and Aqua satellites, which were launched in December 1999 and May 2002, respectively. The Terra satellite has an overpass time around 10 : 30 PM when ascending and 10 : 30 AM when descending. The Aqua satellite's overpass time is roughly 1 : 30 PM when ascending and 1 : 30 AM while descending.

MODIS has been widely used in the field of energy balance studies since it gives a firm footing for spatiotemporally continuous information over the entire surface of the globe [12]. MODIS information from the Terra spacecraft (10 : 30 overpass) is used to estimate ET using various equations. MOD07 having a spatial resolution of 5 km is

Table 1: General characteristics of the study sites.

ID	Latitude	Longitude	Altitude (m)	Temperature (°C)	Precipitation (mm)
Hamheung	39.93°N	127.55°E	13	9.8	890.3
Anju	39.62°N	125.65°E	125	9.2	1072.0
Kimchaek	40.67°N	129.20°E	540	8.4	700.0
Tsetserleg	47.45°N	101.47°E	1695	0.5	336.0
Darkhan	49.47°N	105.98°E	709	−0.6	309.0
Sainshand	44.90°N	110.12°E	915	4.0	119.0
Dalanzadgad	43.58°N	104.42°E	1469	4.6	127.0
Khovd	48.02°N	91.65°E	1405	0.3	119.0
Murun	49.63°N	100.17°E	1288	−1.3	207.0
Darwin	12.46°S	131.05°E	34	27.4	1694
Giles	25.03°S	128.30°E	598	22.7	291.7
Perth	31.88°S	116.13°E	25	18.7	807.0
Brisbane	27.48°S	153.04°E	8	20.3	1168.0
Adelaide	34.87°S	138.87°E	48	16.4	536.0
Melbourne	37.88°S	145.04°E	49	14.8	666.0

chosen among all current MODIS items given by NASA as it incorporates air and dew point temperatures. The MOD07 provides instantaneous geophysical variables such as latitude, longitude, dew point and air temperatures, surface pressure, solar zenith angle, and brightness temperature and total perceptible water vapor with moderate resolution [13, 14]. Together with these geophysical variables, air and dew point temperatures were considered a part of this study. The MODIS cloud product (MOD06) was used for calculation of radiation under cloudy sky conditions. The cloud parameters including cloud fraction, cloud top temperature, and cloud optical thickness with 1 km spatial determination and cloud emissivity with 5 km spatial resolution [15] were used in this study. The sinusoidal projection was implemented to the land products to peruse various needs for major discipline groups: Korean Peninsula placed on horizontal tile numbers 27 to 28 and vertical tile numbers 4 to 5 (H27V04, H27V05, H28V04, and H28V05) in the sinusoidal projection. In the case of Mongolia, the HDF tiles are H23V03, H23V04, H24V03, H24V04, H25V03, H25V04, H26V03, and H26V04. For Australia, the HDF tiles are H27V12, H28V11, H28V12, H29V10, H29V11, H29V12, H30V10, H30V11, H30V12, H31V10, H31V11, and H31V12. The MOD13A2 provides NDVI and the Enhanced Vegetation Index (EVI) at a temporal resolution of 16 days and spatial resolution of 1 km [16], and the MOD15A2 provides Leaf Area Index (LAI) and the Fraction of Photosynthetically Active Radiation (fPAR) for every 8 days. The MOD17A2 provides vegetation information at 1 km spatial resolution in every 8-day intervals through gross primary productivity (GPP) and net primary productivity (NPP) products. Hemispherical reflectance (white sky albedo) and bihemispherical reflectance (black sky albedo) were offered by the MOD43 albedo product. Reflected solar radiation was estimated by using the shortwave infrared band (10th band) of the white sky albedo from the MCD43B3 albedo product [17].

For estimation of SPI, the climatological ground measurement data were obtained from the weather stations. Because SPI is calculated from more than 30 years of data, we have chosen a location that provides over 30 years of precipitation data in Korean Peninsula, Australia, and Mongolia (12 sites from Mongolia: http://worldweather.wmo.int/en/country.html?countryCode=MNG; 32 sites from Australia: http://www.bom.gov.au/climate/data/stations/; 60 sites from Korean Peninsula: http://www.kma.go.kr/weather/climate/past_cal.jsp). The streamflow data were obtained from Global Land Data Assimilation System (GLDAS) for drought status validation [18]. The GLDAS Noah dataset having 25 km spatial resolution and 1-month estimated data were used as the ground basis observation for validation purposes.

3. Methodology

In this study, the following four drought indices were estimated and compared: EWDI, ESI, SPI-3, and VCI. Since selected drought indices have different data ranges, they were normalized for more intuitive comparison with EWDI. Following sections briefly describe the four drought indices.

3.1. Evaporative Stress Index (ESI). ESI is calculated by using AET-PET ratios denoted by f_{PET}:

$$f_{\mathrm{PET}} = \frac{\mathrm{AET}}{\mathrm{PET}}. \tag{1}$$

A well-known Priestley–Taylor algorithm (Priestley and Taylor, 1972) was used for calculations of potential evapotranspiration (PET). For PET calculation, all hydrometeorological data were derived from satellite observations. We modified the algorithm of Cleugh et al. [19] and Mu et al. [17] which estimates AET based on the following Penman–Monteith equation [20]:

$$\lambda E = \frac{\Delta\left(R_{\mathrm{N}} - G\right) + \left(\rho C_{\mathrm{p}}\left(e_{\mathrm{sat}} - e\right)\right)/r_{\mathrm{a}}}{\Delta + \gamma\left(\left(1 + r_{\mathrm{s}}\right)/r_{\mathrm{a}}\right)}, \tag{2}$$

where λE is the latent heat flux ($\mathrm{W{\cdot}m^{-2}}$), λ is the latent heat of vaporization ($\mathrm{J{\cdot}kg^{-1}}$), Δ is the slope of the curve relating the saturated water vapor pressure to temperature ($\mathrm{kPa{\cdot}K^{-1}}$), R_{N} is the net radiation flux ($\mathrm{W{\cdot}m^{-2}}$), G is the soil heat flux ($\mathrm{W{\cdot}m^{-2}}$), ρ is the air density ($\mathrm{kg{\cdot}m^{-3}}$), C_{P} is the

specific heat capacity of air ($J \cdot kg^{-1} \cdot K^{-1}$), e_{sat} is the saturated water vapor pressure (Pa), e is the actual water vapor pressure (Pa), r_a is the aerodynamic resistance ($s \cdot m^{-1}$), γ is the psychrometric constant and is set as a constant with a value of 0.66 Pa K^{-1}, and r_s is the surface resistance ($s \cdot m^{-1}$).

All required parameters of equation (2) were obtained from satellite observations using the algorithms of Cleugh et al. [19] and Mu et al. [17]. In this study, the only difference was EVI instead of NDVI because the EVI might enhance the accuracy of the estimated AET value [17]. This study enhanced the accuracy of the AET estimation by introducing the gross primary productivity (GPP) values for the estimation of the surface resistance (r_s). The GPP can be derived from the MOD17 product, and it is known to precisely reflect the impact of photosynthesis which EVI and NDVI cannot reflect [21]. To enhance the accuracy of the algorithm, this study revised the equation for calculating the vegetation cover fraction by the following equation:

$$F_{cc_i} = \frac{1}{2}\left[\frac{EVI_i - EVI_{min}}{EVI_{max} - EVI_{min}} + \frac{GPP_i - GPP_{min}}{GPP_{max} - GPP_{min}}\right], \quad (3)$$

where F_{cc_i} stands for the ith day's vegetation cover fraction and the subscripts max and min symbolize the maximum and minimum value of all GPP and EVI values attained for all observation periods.

This calculated value of vegetation cover fraction is subsequently used as the input of the set of equations [8] to estimate the surface resistance value (r_s) to be used in equation (2). Figure 2 shows the comparison among the AET values estimated based on the method of this study (y) to the reference flux tower ET value (x) at Cheongmicheon (CFC) and Seolmacheon (SMC) gages located in Korean Peninsula. The AET value based on the method of Mu et al. [17] is shown for comparison. It can be noted that the method of this study has greater accuracy compared to the method of Mu et al. [17] in terms of correlation coefficient (Figure 2).

Lastly, the Evaporative Stress Index (ESI) is obtained by normalizing the estimated f_{PET} value:

$$ESI = \frac{f_{PET} - \mu_{f_{PET}}}{\sigma_{f_{PET}}}, \quad (4)$$

where $\mu_{f_{PET}}$ and $\sigma_{f_{PET}}$ represent the mean and the standard deviation of all f_{PET} values estimated for the entire study period at a given grid cell location.

3.2. Energy-Based Water Deficit Index (EWDI). The water status of the land surface under different conditions can be estimated by considering the EWDI which represents the water deficit condition. Based on apparent thermal inertia (ATI), the EWDI was corporated using the ESI and Soil Moisture Saturation Index (SMSI). The ATI evaluates the spatiotemporal variability of soil moisture and is derived directly from multispectral satellite imageries [22].

Using the differences in land surface temperature (ΔLST) and land surface albedo, the ATI is calculated as follows:

$$ATI = \frac{1 - \alpha}{\Delta LST},$$
$$Z(ATI)_{i,j} = SMSI = \frac{ATI_{i,j} - ATI_{min}}{ATI_{max} - ATI_{min}}, \quad (5)$$

where α represents the land surface albedo and ΔLST is the diurnal land surface temperature, which is the difference of temperature between the daytime and nighttime. Since the ATI represents the sum of canopy and soil moisture variability, the higher the value, the higher the soil water content of the land surface [22, 23]. ATI values are normalized by using SMSI for the purpose of calculating EWDI. $ATI_{i,j}$ represents the ATI value at the ith latitude and jth longitude.

After calculation of the EWDI, the ESI and SMSI terms are differences in the standardized anomaly:

$$EWDI_{i,j} = Z\left(ESI_{i,j} + SMSI_{i,j}\right)_{i,j}, \quad (6)$$

where the EWDI is a dimensionless index ranging from infinite negative values (drier than normal) to infinite positive values (wetter than normal). Surface albedo products (MCD43B3) in 8 days were used in this study. Leaf Area Index (MOD15A2), NDVI and EVI (from the MOD13A2 product), and atmospheric products (MOD07_L2 atmosphere product) were used for calculating EWDI.

3.3. Standardized Precipitation Index (SPI). The SPI was established by McKee et al. [24]. The SPI is assessed by using the monthly average precipitation dataset, for a continuous period of at least 30 years. Because SPI is calculated from more than 30 years of data, we have chosen a location that provides over 30 years of monthly precipitation data. The SPI uses monthly precipitation aggregated at various time scales (1 month, 3 months, 6 months, 12 months, etc.). In general, gamma fitting function is applied for each dataset to describe probability interactions. The distinction of the SPI is that it does not depend upon the model. A straightforward valuation of precipitation is the input, disparate with the PDSI, which makes assumptions about water storage and deficit.

3.4. Vegetation Condition Index (VCI). The Vegetation Condition Index (VCI hereafter) [1] is the most widely used satellite-based drought index to monitor vegetation conditions. VCI is determined based on the Normalized Difference Vegetation Index (NDVI) which assesses live green vegetation for the observed target. VCI is determined using the following equation:

$$VCI = Z\left[\frac{NDVI - NDVI_{min}}{NDVI_{max} - NDVI_{min}}\right], \quad (7)$$

where NDVI, $NDVI_{min}$, and $NDVI_{max}$ are the smoothed monthly normalized difference vegetation index at a given grid cell location, its multiyear maximum, and its multiyear minimum, respectively, and Z is the meaning of standardized normalization. Since the VCI is an index value which normalizes the value varying between 0 and 1,

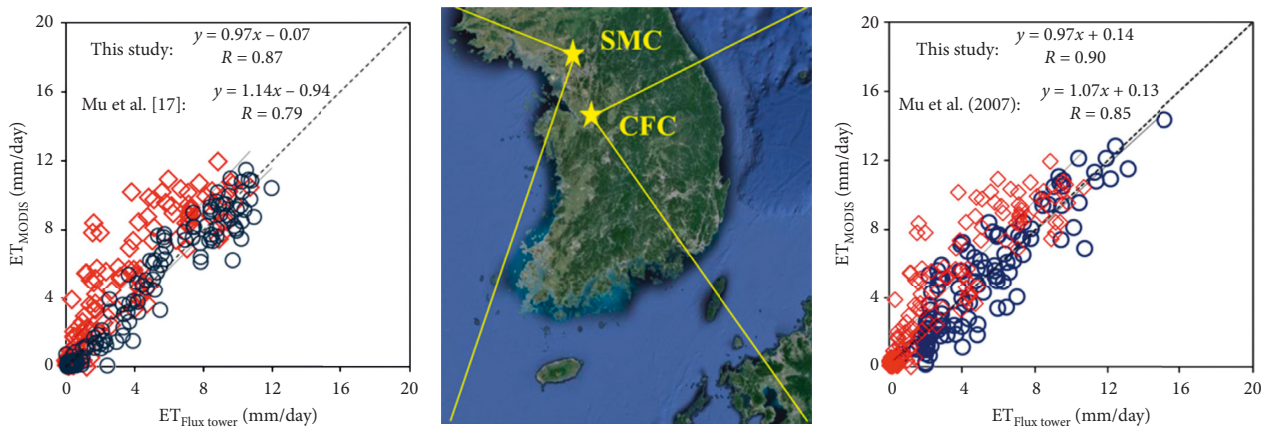

Figure 2: Comparison of the actual evapotranspiration estimated by the method of this study.

Table 2: Error matrix result for Korean Peninsula (Hamheung site) during 2001–2010.

Hamheung	Streamflow		Sum	Drought accuracy (%)	Overall accuracy (%)
	Drought	No drought			
Moderate drought ($Streamflow_{lower\ quartile}$ = 0.03137 cfs)					
ESI					
Drought	54	4	58	54/58 = 93.10	110/120 = 91.67
No drought	6	56	62		
Sum	60	60	120		
EWDI					
Drought	54	3	57	54/57 = 94.74	113/120 = 94.17
No drought	4	59	63		
Sum	58	62	120		
SPI-3					
Drought	45	7	52	45/52 = 86.54	100/120 = 83.33
No drought	13	55	68		
Sum	58	62	120		
VCI					
Drought	35	18	53	35/53 = 66.04	85/120 = 70.83
No drought	17	50	67		
Sum	52	68	120		

Table 3: Error matrix result for Australia (Brisbane site) during 2001–2010.

Brisbane	Streamflow		Sum	Drought accuracy (%)	Overall accuracy (%)
	Drought	No drought			
Moderate drought ($Streamflow_{lower\ quartile}$ = 0.04784 cfs)					
ESI					
Drought	45	7	52	45/52 = 86.54	100/120 = 83.33
No drought	13	55	68		
Sum	58	62	120		
EWDI					
Drought	54	3	57	54/57 = 94.74	113/120 = 94.17
No drought	4	59	63		
Sum	58	62	120		
SPI-3					
Drought	39	17	56	39/56 = 69.64	84/120 = 70.00
No drought	19	45	64		
Sum	58	62	120		
VCI					
Drought	29	28	57	29/57 = 50.88	91/120 = 75.83
No drought	1	62	63		
Sum	30	90	120		

Table 4: Error matrix result for Mongolia (Tsetserleg site) during 2001–2010.

Tsetserleg	Streamflow		Sum	Drought accuracy (%)	Overall accuracy (%)
	Drought	No drought			
Moderate drought ($Streamflow_{lower\ quartile}$ = 0.04314 cfs)					
ESI					
Drought	45	7	52	45/52 = 86.54	100/120 = 83.33
No drought	13	55	68		
Sum	58	62	120		
EWDI					
Drought	54	3	57	54/57 = 94.74	113/120 = 94.17
No drought	4	59	63		
Sum	58	62	120		
SPI-3					
Drought	39	17	56	39/56 = 69.64	84/120 = 70.00
No drought	19	45	64		
Sum	58	62	120		
VCI					
Drought	17	33	50	17/50 = 34.00	74/120 = 61.67
No drought	13	57	70		
Sum	30	90	120		

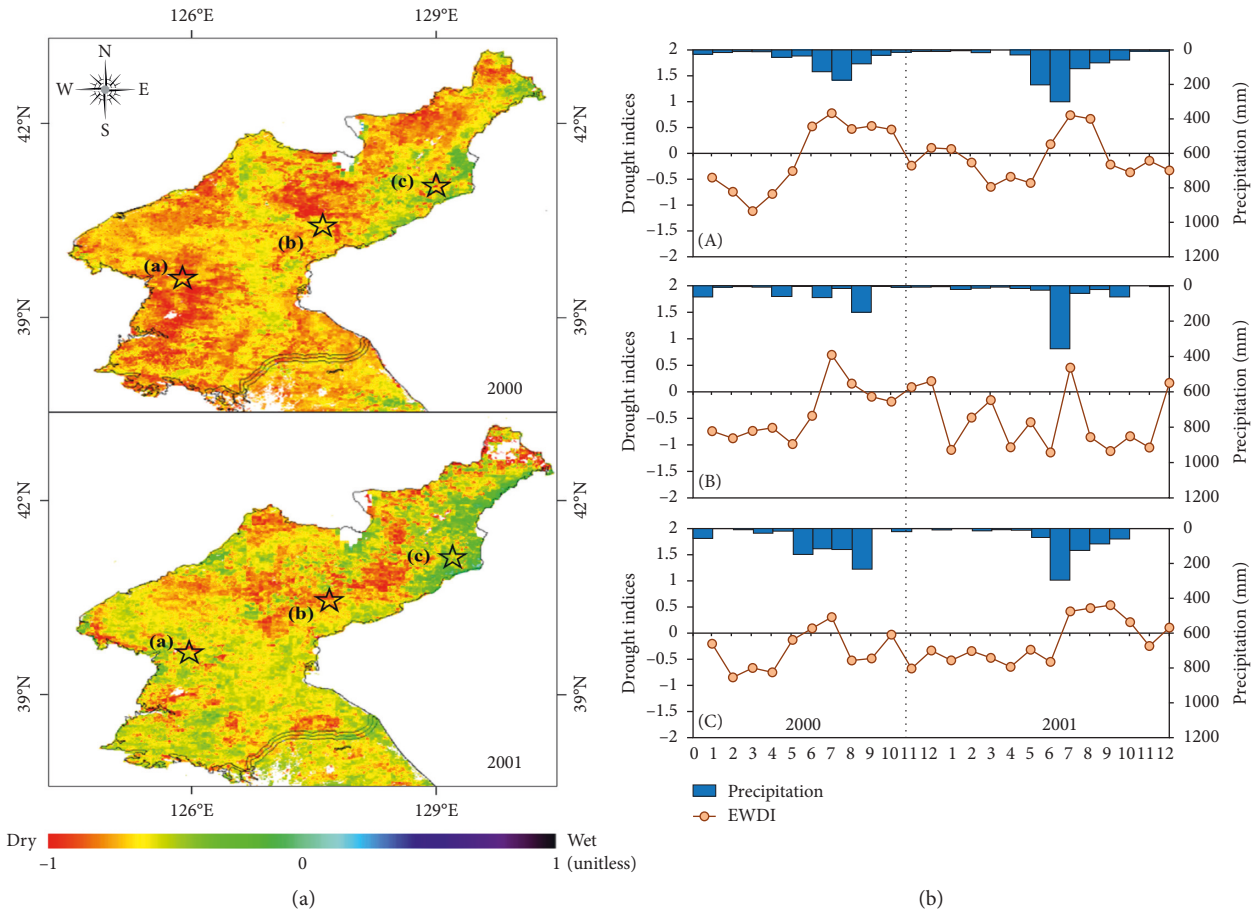

(a) (b)

Figure 3: (a) Spatial distributions of EWDI for 2000 and 2001 in North Korea; (b) temporal distributions of EWDI and precipitation in the (A) Anju, (B) Hamheung, and (C) Kimchaek sites.

approximately 95 percent of the VCI at a given grid cell location varies from −2 (harsh drought) to 2 (healthy vegetation condition).

3.5. Error Matrix Method. To correctly detect the drought event and severity, numerous drought indices were evaluated using an error matrix method [25, 26]. An error

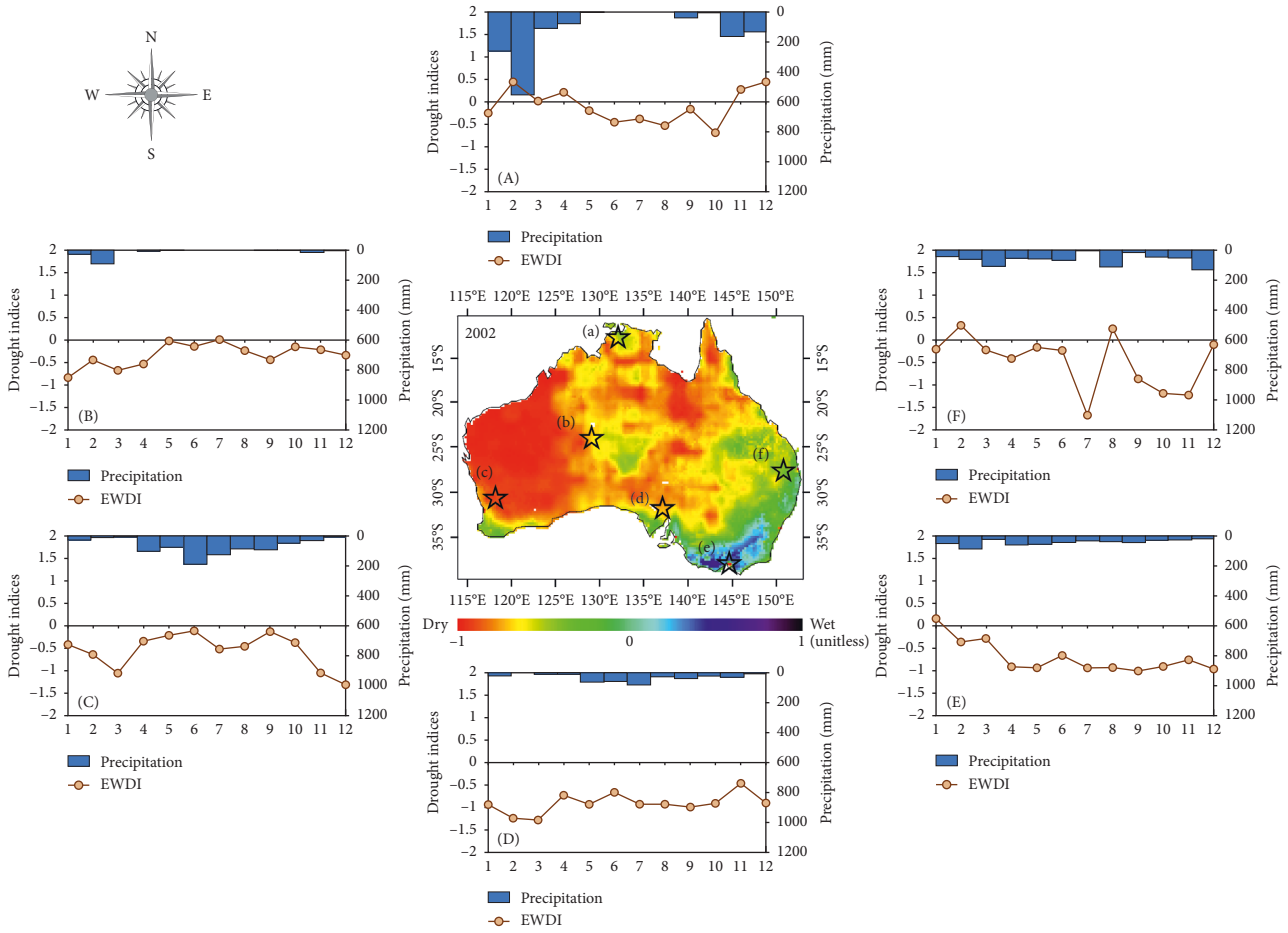

Figure 4: Spatial distributions of EWDI for 2002 in Australia (central part); temporal distributions of EWDI and precipitation in the (A) Darwin, (B) Giles, (C) Perth, (D) Adelaide, (E) Melbourne, and (F) Brisbane sites (external parts).

matrix method is a formed array that consists of drought or wet condition as compared to the category of drought suggested by the observation data such as streamflow and soil moisture. When the value of the standardized streamflow is less than 0, it is defined as a drought status. The fallouts of matrix are represented to obtain the accuracy of drought, and the accuracy of drought is the ratio of all observation datasets that are certificated as drought by both the index and the observation datasets to the total number of drought statuses.

4. Results and Discussions

4.1. Analysis of Drought Accuracy Using Error Matrix Method. Error matrix derived from GLDAS streamflow dataset in Tables 24 showed overall accuracy from 75 to 92%, with approximately 90% accuracy during dry season. This result indicates that all four drought indices (EWDI, ESI, VCI, and SPI-3) have a good degree of reliability for analyzing the drought status at each site. The applicability of the EWDI was best compared to that of another drought index under drought conditions. For streamflow, the EWDI and ESI had markedly better results than did the VCI and SPI-3, with drought and overall accuracies ranging between 75% and 90% at every study site. The patterns of SPI-3 were relatively slow because it related to the precipitation variation.

These intercomparison fallouts prove the applicability of the satellite-based drought indices and the impact of drought on streamflow [25]. However, some limitations may exist. As noted by Karnieli et al. [27] and Choi et al. [25], the vegetation-based drought indices such as the VCI and Evapotranspiration-Based Drought Index (ESI) might be less appropriate for the time and the places where drought conditions cannot be fully represented by vegetation conditions such as dormant season and the area with high latitudes and elevations. For the aforementioned results, the EWDI precisely predicts the drought status, compared to the SPI-3. The EWDI, ESI, VCI, and SPI-3 were good indices of extreme drought status.

4.2. Spatiotemporal Patterns of Various Drought Indices. In Section 4.2, the spatiotemporal patterns of EWDI and actual drought situations were compared. In the case of North Korea, several previous studies have reported that there has been a serious drought situation from February to May in 2000 and from March to June in 2001, respectively [28–30]. Jang et al. [28] examined the cases of drought

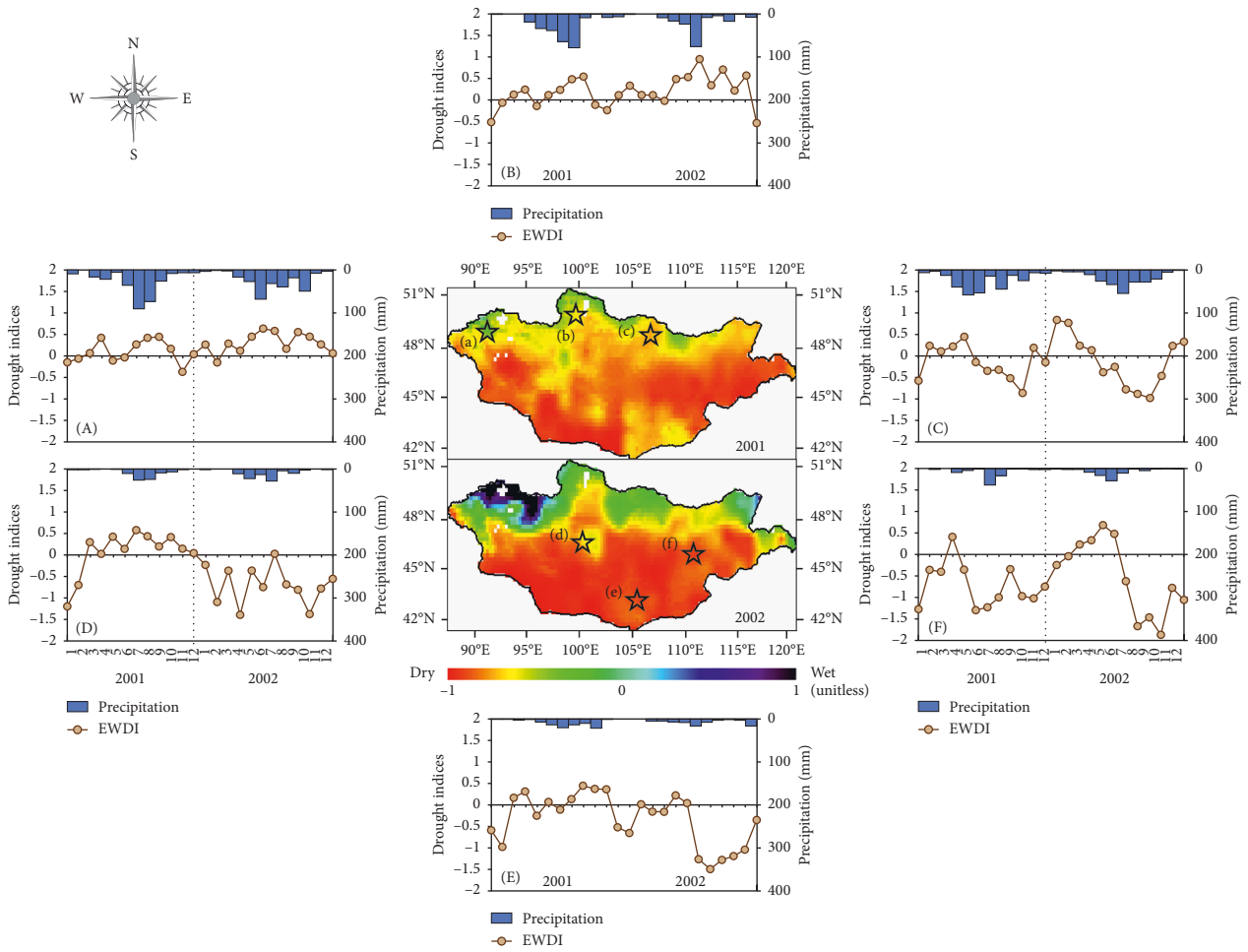

FIGURE 5: Spatial distributions of EWDI for 2001 and 2002 in Mongolia (central part); temporal distributions of EWDI and precipitation in the (A) Khovd, (B) Murun, (C) Darkhan, (D) Tsetserleg, (E) Dalanzadgad, and (F) Sainshand sites (external parts).

damage in North Korea from 2000 to 2001 and showed the spatial distribution of drought damage regions. Nam et al. [30] reported that severe drought conditions occurred in the western part of North Korea in 2000 and in the eastern part of North Korea in 2001.

Figure 3 represents the annual mean spatial distributions of EWDI for 2000 and 2001 in North Korea. It also shows the temporal distribution of EWDI and precipitation in the Anju, Hamheung, and Kimchaek sites.

Comparing the results of this study with those of previous studies, it can be seen that a more severe drought condition occurred during 2000 than 2001 at Anju, which is located in the western part of North Korea. On the contrary, in Kimchaek and Hamheung areas located in the eastern part of the country, a more severe drought occurred in 2001 than in 2000. The main reason of this phenomenon can be explained by the lack of precipitation. In 2000, the amount of precipitation in the western region was 20% of that in the normal year, while in 2001, precipitation in the eastern region was only 17% lower than that in the normal year. For this reason, the spatial distribution of drought was shown differently by year [30].

In the case of Australia, Horridge et al. [31] reported that there has been a serious drought situation from April to December 2002. Horridge et al. [31] showed the cases of drought damage in Australia in 2002 and reported the spatial distribution of drought damage regions.

Figure 4 represents the annual mean spatial distributions of EWDI for 2002 in Australia. It also shows the temporal distribution of EWDI and precipitation in the Darwin, Giles, Perth, Adelaide, Melbourne, and Brisbane sites. Among the six validation sites, Perth had the lowest annual average precipitation of 688 mm in 2002, which was 32% lower than that in the normal year [31]. The value of the drought index for that period indicated the drought status. In the case of the Darwin site, there was an extreme drought situation from April to August, but there was a lot of precipitation during the rest of the year. For this reason, the annual average drought condition was expressed moderately (Figure 4).

Finally, in the case of Mongolia, several previous researches have reported that there has been a serious drought situation from February to October 2001 and from March to December 2002, respectively [32, 33]. Bayarjargal et al. [32] examined the cases of drought damage in Mongolia in 2001 and 2002. They reported that the overall drought condition was serious in 2001, but in 2002, there was extreme drought condition in the southern region.

Davi et al. [33] showed the spatial distribution of drought condition regions.

Figure 5 represents the annual mean spatial distributions of EWDI for 2001 and 2002 in Mongolia. It also shows the temporal distributions of EWDI and precipitation in the Khovd, Murun, Darkhan, Tsetserleg, Dalanzadgad, and Sainshand sites. Among the six validation sites, the Dalanzadgad site had the lowest annual average precipitation of 95 mm in 2001 and 76 mm in 2002, which were 58% lower than that in the normal year [32]. The value of the drought index for that period also indicated the drought status. In the case of the Khovd and Murun sites, there were extreme drought situations from February to April, but there was a lot of precipitation during the rest of the year. For this reason, the annual average drought condition was expressed moderately (Figure 5).

5. Conclusions

In this study, conventional and satellite-based drought indices were compared over drought-vulnerable sites (Korean Peninsula, Mongolia, and Australia) from 2000 to 2010. The EWDI showed the highest drought accuracy through the error matrix method (drought accuracy ranged from 85.71 to 94.74%; Hamheung in North Korea, Brisbane in Australia, and Tsetserleg in Mongolia: 94.74%).

The applicability of the EWDI was determined by comparing the estimated EWDI with actual drought conditions. The results of the EWDI and the spatiotemporal distribution of the actual drought situation showed a similar tendency. In the case of North Korea, there has been a serious drought situation from February to May in 2000 and from March to June in 2001, respectively. More severe drought condition occurred during 2000 than 2001 at the Anju region, which is located in the western part of North Korea. On the one hand, in Kimchaek and Hamheung areas located in the eastern part of the country, a more severe drought occurred in 2001 than in 2000. In the case of Australia, there has been a serious drought situation from April to December 2002. The most severe droughts in Perth were examined because the precipitation was only about 32% lower than that in the normal year. On the other hand, Darwin was relatively less drought prone due to heavy rainfall during the summer season (from September to March). Finally, in the case of Mongolia, there has been a serious drought situation from February to October 2001 and from March to December 2002, respectively. During the drought period, the most serious droughts occurred in the Dalanzadgad region and the less severe drought conditions in the Khovd and Murun regions.

Through the above-mentioned results, the applicability of EWDI was good compared to that of the other drought indices. Based on the results, RS-based indices were identified as good indicators for detecting the drought status especially when climate data were not available or were sparsely distributed.

Data Availability

The data used to support the findings of this study are available from the corresponding author upon request.

Conflicts of Interest

The authors declare that they have no conflicts of interest.

Acknowledgments

This research was supported by Basic Science Research Program through the National Research Foundation of Korea (NRF) funded by the Ministry of Science, ICT and Future Planning (2018R1C1B6008805) and the Ministry of Education, Science and Technology (Project No. NRF-2017R1C1B2003927).

References

[1] F. N. Kogan, "Droughts of the late 1980s in the United States as derived from NOAA polar-orbiting satellite data," *Bulletin of the American Meteorological Society*, vol. 76, no. 5, pp. 655–668, 1995.

[2] F. N. Kogan, "Global drought watch from space," *Bulletin of the American Meteorological Society*, vol. 78, no. 4, pp. 621–636, 1997.

[3] M. C. Anderson, J. Norman, J. Mecikalski, J. Otkin, and W. P. Kustas, "A climatological study of evapotranspiration and moisture stress across the continental United States based on thermal remote sensing: 1. Model formulation," *Journal of Geophysical Research: Atmospheres*, vol. 112, no. 10, 2007.

[4] M. C. Anderson, J. Norman, J. Mecikalski, J. Otkin, and W. P. Kustas, "A climatological study of evapotranspiration and moisture stress across the continental United States based on thermal remote sensing. 2. Surface moisture climatology," *Journal of Geophysical Research*, vol. 112, no. 11, 2007.

[5] M. C. Anderson, C. Hain, B. Wardlow, A. Pimstein, J. R. Mecikalski, and W. P. Kustas, "Evaluation of drought indices based on thermal remote sensing of evapotranspiration over the continental United States," *Journal of Climate*, vol. 24, no. 8, pp. 2025–2044, 2011.

[6] Q. Mu, M. Zhao, J. S. Kimball, N. G. McDowell, and S. W. Running, "A remotely sensed global terrestrial drought severity index," *Bulletin of the American Meteorological Society*, vol. 94, no. 1, pp. 83–98, 2013.

[7] M. R. Keshavarz, M. Vazifedoust, and A. Alizadeh, "Drought monitoring using a soil wetness deficit index (SWDI) derived from MODIS satellite data," *Agricultural Water Management*, vol. 132, pp. 37–45, 2014.

[8] C. Sur, J. Hur, K. Kim, W. Choi, and M. Choi, "An evaluation of satellite-based drought indices on a regional scale," *International Journal of Remote Sensing*, vol. 36, no. 22, pp. 5593–5612, 2015.

[9] P. Batima, *Climate Change Vulnerability and Adaptation in the Livestock Sector of Mongolia: A Final Report Submitted Assessments of Impacts and Adaptations to Climate Change (AIACC)*, The International Start Secretariat, Washington, DC, USA, 2006.

[10] T. Sato, F. Kimura, and A. Kitoh, "Projection of global warming onto regional precipitation over Mongolia using a regional climate model," *Journal of Hydrology*, vol. 333, no. 1, pp. 144–154, 2007.

[11] K. Hwang, M. Choi, S. O. Lee, and J.-W. Seo, "Estimation of instantaneous and daily net radiation from MODIS data under clear sky conditions: a case study in East Asia," *Irrigation Science*, vol. 31, pp. 1173–1184, 2013.

[12] B. Tang and Z. Li, "Estimation of instantaneous net surface longwave radiation from MODIS cloud-free data," *Remote Sensing of Environment*, vol. 112, no. 9, pp. 3482–3492, 2008.
[13] W. P. Menzel, S. W. Seemann, J. Li, and L. E. Gumley, *MODIS Atmospheric Profile Retrieval Algorithm Theoretical Basis Document (MOD07)*, University of Winconsin-Madison Press, Madison, WI, USA, 2002.
[14] S. W. Seemann, J. Li, W. P. Menzel, and L. E. Gumley, "Operational retrieval of atmospheric temperature, moisture, and ozone from MODIS infrared radiances," in *Journal of Applied Meteorology*, vol. 42, pp. 1072–1091, 2003.
[15] G. Bisht and R. L. Bras, "Estimation of net radiation from the MODIS data under all sky conditions: southern great plains case study," *Remote Sensing of Environment*, vol. 114, pp. 1522–1534, 2010.
[16] A. R. Huete, K. Didan, T. Miura, E. P. Rodriguez, X. Gao, and L. G. Ferreira, "Overview of the radiometric and biophysical performance of the MODIS vegetation indices," *Remote Sensing of Environment*, vol. 83, no. 1-2, pp. 195–213, 2002.
[17] Q. Mu, F. A. Heinsch, M. Zhao, and S. W. Running, "Development of a global evapotranspiration algorithm based on MODIS and global meteorology data," *Remote Sensing of Environment*, vol. 111, no. 4, pp. 519–536, 2007.
[18] M. Rodell, P. R. Houser, U. Jambor et al., "The global land data assimilation system," *Bulletin of the American Meteorological Society*, vol. 85, no. 3, pp. 381–394, 2004.
[19] H. A. Cleugh, R. Leuning, Q. Mu, and S. W. Running, "Regional evaporation estimates from flux tower and MODIS satellite data," *Remote Sensing of Environment*, vol. 106, no. 3, pp. 285–304, 2007.
[20] J. L. Monteith, "Evaporation and environment," *Symposia of the Society for Experimental Biology*, vol. 19, pp. 205–234, 1965.
[21] W. Yuan, S. Liu, G. Yu et al., "Global estimates of evapotranspiration and gross primary production based on MODIS and global meteorology data," *Remote Sensing of Environment*, vol. 114, no. 7, pp. 1416–1431, 2010.
[22] W. W. Verstraeten, F. Veroustraete, C. J. van der Sande, I. Grootaers, and J. Feyen, "Soil moisture retrieval using thermal inertia, determined with visible and thermal spaceborne data, validated for European forests," *Remote Sensing of Environment*, vol. 101, no. 3, pp. 299–314, 2006.
[23] T. Y. Chang, Y. C. Wang, C. C. Feng, A. D. Ziegler, T. W. Giambelluca, and Y. A. Liou, "Estimation of root zone soil moisture using apparent thermal inertia with MODIS imagery over a tropical catchment in Northern Thailand," *IEEE Journal of Selected Topics in Applied Earth Observations and Remote Sensing*, vol. 5, no. 3, pp. 752–761, 2012.
[24] T. B. McKee, N. J. Doesken, and J. Kleist, "The relationship of drought frequency and duration to time scales," in *Proceedings of the Preprints of the 8th Conference on Applied Climatology*, vol. 17–22, pp. 179–184, Anaheim, CA, USA, January 1993.
[25] M. Choi, J. M. Jacobs, M. C. Anderson, and D. D. Bosch, "Evaluation of drought indices via remotely sensed data with hydrological variables," *Journal of Hydrology*, vol. 476, pp. 265–273, 2013.
[26] R. G. Congalton, "A review of assessing the accuracy of classifications of remotely sensed data," *Remote Sensing of Environment*, vol. 37, no. 1, pp. 35–46, 1991.
[27] A. Karnieli, N. Agam, and R. T. Pinker, "Use of NDVI and land surface temperature for drought assessment: merits and limitations," *Journal of Climate*, vol. 23, no. 3, pp. 618–633, 2010.
[28] M. W. Jang, S. H. Yoo, and J. Y. Choi, "Analysis of spring drought using NOAA/AVHRR NDVI for North Korea," *Journal of the Korean Society of Agricultural Engineers*, vol. 49, no. 6, pp. 21–33, 2007.
[29] S. U. Kang and J. W. Moon, "Drought analysis using SC-PDSI and derivation of drought severity-duration-frequency curves in North Korea," *Journal of Korea Water Resources Association*, vol. 47, no. 9, pp. 813–824, 2014.
[30] W. H. Nam, S. H. Yoo, M. W. Jang, and J. Y. Choi, "Application of meteorological drought indices for North Korea," *Journal of the Korean Society of Agricultural Engineers*, vol. 50, no. 3, pp. 3–15, 2008.
[31] M. Horridge, J. Madden, and G. Wittwer, "Using a highly disaggregated multi-regional single-country model to analyse the impacts of the 2002-03 drought on Australia," *Journal of Policy Modelling*, vol. 27, pp. 285–308, 2005.
[32] A. Bayarjargal, A. Karnieli, M. Bayasgalan, S. Khudulmur, C. Gandusha, and T. J. Tucker, "A comparative study of NOAA–AVHRR derived drought indices using change vector analysis," *Remote Sensing of Environment*, vol. 105, no. 1, pp. 9–22, 2006.
[33] N. K. Davi, G. C. Jacoby, R. D. D'Arrigo, N. Baatarbileg, L. Jinbao, and A. E. Curtis, "A tree-ring-based drought index reconstruction for far-Western Mongolia: 1565–2004," *International Journal of Climatology*, vol. 29, no. 10, pp. 1508–1514, 2009.